Tumble-Vortex Core Line Extraction

Philipp Jung
Heidelberg University
Philipp.Jung@iwr.uni-heidelberg.de

Philip Hausner
Heidelberg University
Philip.Hausner@iwr.uni-heidelberg.de

Lukas Pilz
Heidelberg University
Lukas.Pilz@iwr.uni-heidelberg.de

Julien Stern
Heidelberg University
Julien.Stern@iwr.uni-heidelberg.de

Christian Euler
University of Mainz
eulerc@uni-mainz.de

Michael Riemer
University of Mainz
mriemer@uni-mainz.de

Filip Sadlo
Heidelberg University
sadlo@uni-heidelberg.de

***Abstract*—In this paper, we focus on the extraction of vortex core lines from 3D vector fields containing tumble vortices, i.e., vortices with vanishing longitudinal velocity component. While there exist many different definitions for vortex core lines, these are typically formulated and extracted by means of the parallel vectors operator, i.e., as those points in space where two (derived) vector fields are parallel or antiparallel. However, in case of vanishing longitudinal component and other degeneracies which we investigate, the existing approaches to solve the parallel vectors problem tend to fail. We present a technique to solve these cases, based on subdivision and problem transformation, and examine and exemplify our technique by means of an analytical vortex model and data from computational fluid dynamics.**

I. Introduction

Vortical motion in flow fields is hard to grasp. Although a multitude of vortex definitions has been proposed, a generic formulation is missing—necessitating explorative visual analysis based on advanced visualization techniques. One subject in such explorations is the choice of the appropriate definition.

Vortex visualization can be divided into two groups: visualization by means of *vortex criteria*, i.e., fields that indicate the volumetric presence of a vortex, and by reduced representations, such as vortex hulls and *vortex core lines*. Vortex core lines, i.e., the generally curved axes (or "centerlines") of vortices, are widely used because they provide a concise representation at little occlusion, and can serve for seeding streamlines to visualize the flow through the vortex.

Many vortex core line concepts can be formulated by means of (anti-)parallelism of two vector fields. A widely used example is the definition by Sujudi and Haimes [1], which, in the formulation due to Peikert and Roth [2], identifies those points $\mathbf{x}$ in space as being part of the vortex core line where velocity $\mathbf{u}(\mathbf{x})$ is (anti-)parallel to the acceleration $\mathbf{a}(\mathbf{x}) := (\nabla\mathbf{u}(\mathbf{x}))\mathbf{u}(\mathbf{x})$, i.e., in short notation $\mathbf{u} \parallel \mathbf{a}$. In their parallel vectors (PV) operator [2], Peikert and Roth presented an approach to find these solution curves by identifying their intersections with the faces of the data grid. To determine these intersections on quad faces of the grid, they presented two alternatives: an eigenvector-based approach necessitating the subdivision of the quad into two triangles, and an approach based on Newton iterations within the quad. Because Newton iterations can miss solutions, we constrain our analysis to the eigenvector-based approach in this paper. As we exemplify below, the eigenvector-based approach is quite robust in general, but typically fails if the flow velocity component along the core line vanishes, also denoted tumble vortex.

Such tumble vortices can appear in analytical vortex models, but they can also be encountered in flow simulations with symmetry conditions. As we detail below, there are several reasons that cause at least partial failure of the PV solution strategy by Peikert and Roth. We provide both an analysis of the reasons for its failure, and use that to motivate respective solutions, which comprises our technical contribution.

II. Related Work

Besides the Sujudi-Haimes criterion [1], there is a multitude of definitions for vortex core lines. Weinkauf et al. [3] and Fuchs et al. [4] present formulations that take into account the time-dependency of vector fields. Levy et al. [5] require $\mathbf{u}(\mathbf{x})$ being (anti-)parallel to vorticity $\nabla \times \mathbf{u}(\mathbf{x})$. Sahner et al. [6] extract them as valley lines of the λ_2-criterion [7]. Valley lines, which can be obtained as height ridge lines [8] of the negated field, represent "generalized" local minima in a scalar field, i.e., local minima in d-dimensional cross-sections of the original domain $\Omega \in \mathbb{R}^n$, with $d < n$. Ridge lines and valley lines of a scalar field $s(\mathbf{x})$ can, according to Peikert and Roth [2], be also extracted by means of the parallel vectors operators, by requiring $\mathbf{g} \parallel \mathbf{Hg}$, with gradient $\mathbf{g} := \nabla s$ and Hessian $\mathbf{H} := \nabla\mathbf{g}$. The $\mathbf{g} \parallel \mathbf{Hg}$ formulation is called implicit, because it does, in contrast to Eberly's original formulation [8], not extract the eigenvectors of $\mathbf{H}$ explicitly. Nevertheless, the solutions of $\mathbf{g} \parallel \mathbf{Hg}$ contain ridge lines, valley lines, and false positives, and the solutions thus need to be filtered accordingly.

There is only comparably few previous work on the solution of the parallel vectors problem itself. Pagot et al. [9] present an approach to obtain PV solutions from discontinuous Galerkin data. Ju et al. [10] provide a parity test for the number of PV intersections per cell face. In this paper, we focus on the determination of the PV face intersections for cases where the eigenvector-based approach by Peikert and Roth [2] fails.

III. Method

We will motivate and present our approach by evaluating the existing eigenvector-based approach by Peikert and Roth at the

example of $\mathbf{u} \parallel \mathbf{a}$, by means of the following vortex model:

$$\mathbf{u}(\mathbf{x}) = \mathbf{R}\,\mathbf{R}_\eta\,\boldsymbol{\nu}\big(\boldsymbol{\phi}^{-1}(\mathbf{x})\big)\ , \tag{1}$$

with

$$\boldsymbol{\phi}^{-1}(\mathbf{x}) = \mathbf{R}^{-1}\begin{pmatrix} x - c_x \\ y - c_y \\ z - c_z \end{pmatrix} \tag{2}$$

being the inverse coordinate transformation (from physical coordinates $\mathbf{x} := (x, y, z)^\top$ to computational coordinates $\boldsymbol{\xi} := (\xi, \eta, \zeta)^\top$) that rotates the field in physical space around rotation center $\mathbf{c} := (c_x, c_y, c_y)^\top$ by the rotation matrix $\mathbf{R}$,

$$\boldsymbol{\nu}(\boldsymbol{\xi}) = \begin{pmatrix} -\omega\eta \\ \omega\xi \\ \lambda_2\zeta^2 + \lambda_1\zeta + \lambda_0 \end{pmatrix} \tag{3}$$

being a rigid body rotation around the ζ-axis with angular velocity ω and longitudinal component $\lambda_2\zeta^2 + \lambda_1\zeta + \lambda_0$ in ζ-direction, and

$$\mathbf{R}_\eta = \begin{pmatrix} \cos\sigma & 0 & \sin\sigma \\ 0 & 1 & 0 \\ -\sin\sigma & 0 & \cos\sigma \end{pmatrix} \tag{4}$$

being a rotation in computational space about the η-axis that shears the vector field by angle σ, with $\sigma = 0$ representing no shear, i.e., $\sigma = 0$ together with $\lambda_0 = \lambda_1 = \lambda_2 = 0$ leads to vortical motion on planes perpendicular to the vortex core line (see Figure 1(a)).

In our experiments, we use

$$\mathbf{R} = \begin{pmatrix} a_x & b_x & \delta_x \\ a_y & b_y & \delta_y \\ a_z & b_z & \delta_z \end{pmatrix}\ , \tag{5}$$

which rotates the ζ-axis to the unit direction vector $\boldsymbol{\delta} := (\delta_x, \delta_y, \delta_z)^\top$ in physical space, with unit vector $\mathbf{b}$ being some vector orthogonal to $\boldsymbol{\delta}$, and $\mathbf{a} := \mathbf{b} \times \boldsymbol{\delta}$.

A. PV Solution by Eigenvectors [2]

In their eigenvector-based approach [2], Peikert and Roth decompose quad faces into two triangles, and search for the position in each triangle where the two vector fields $\mathbf{v}$ and $\mathbf{w}$ are parallel as follows. Since barycentric interpolation is linear, $\mathbf{v}$ can be written by means of a 3 by 3 matrix $\mathbf{V}$ (which computes from the vectors of the field $\mathbf{v}$ at the triangle vertices) and local coordinates s, t as follows:

$$\mathbf{v} = \mathbf{V}\begin{pmatrix} s \\ t \\ 1 \end{pmatrix}\ , \tag{6}$$

with s and t representing, without loss of generality, the barycentric coordinates $\alpha_1 = s$, $\alpha_2 = t$, and $\alpha_3 = 1 - s - t$. Analogously, with the same coordinates, this holds for the vector field $\mathbf{w}$ and its representation with $\mathbf{W}$. According to Peikert and Roth, the parallelism requirement leads to

$$\mathbf{V}\begin{pmatrix} s \\ t \\ 1 \end{pmatrix} = \lambda\mathbf{W}\begin{pmatrix} s \\ t \\ 1 \end{pmatrix}\ , \tag{7}$$

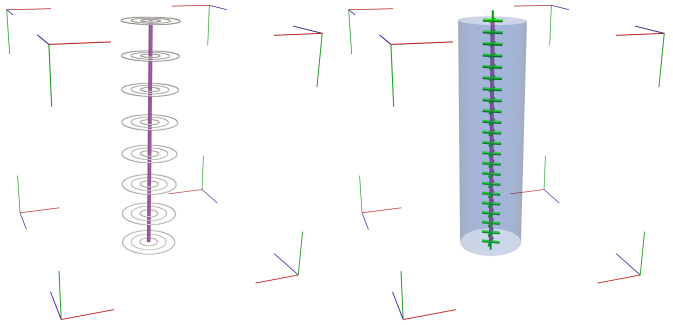

(a) (b)

Fig. 1. Straight vortex aligned with z-axis, with zero longitudinal component, with streamlines (white), and ground-truth core line (purple). (a) Eigenvector-based approach fails, and zero-isolevel isosurfaces of $\mathbf{u} \times \mathbf{a}$ do not exist. (b) Isosurface of z-component of $\mathbf{u} \times \mathbf{a}$ at isolevel -2 (blue) indicates ridge line, which our technique ($\tau_\sigma = 10$) is able to obtain (green crosses). Please note that we depict ridge/valley PV solutions in green throughout this paper.

which, if $\mathbf{W}$ is invertible, solves as

$$\mathbf{W}^{-1}\mathbf{V}\begin{pmatrix} s \\ t \\ 1 \end{pmatrix} = \lambda\begin{pmatrix} s \\ t \\ 1 \end{pmatrix}\ , \tag{8}$$

by an eigenvector problem $\mathbf{M}\mathbf{x} = \lambda\mathbf{x}$ with $\mathbf{M} := \mathbf{W}^{-1}\mathbf{V}$. If $\mathbf{W}$ is not invertible but $\mathbf{V}$ is, one multiplies analogously with $\mathbf{V}^{-1}$, and otherwise no solution exists. We denote this way to solve the PV problem the eigenvector-based approach.

B. PV Solution by Extraction of Valleys and Ridges

In our first test, we set $\mathbf{c} = (0, 0, 0)^\top$, $\boldsymbol{\delta} = (0, 0, 1)^\top$, $\omega = 1$, $\lambda_0 = \lambda_1 = \lambda_2 = 0$, and $\sigma = 0$, i.e., we have a z-axis aligned straight vortex with angular velocity 1, vanishing longitudinal component, and no shear. We discretize the field on a grid of $22 \times 22 \times 22$ nodes with an extent of $[0, 10] \times [0, 10] \times [0, 10]$.

Applying the eigenvector-based approach to the $\mathbf{u} \parallel \mathbf{a}$ criterion for this field ($\mathbf{v} = \mathbf{u}$ and $\mathbf{w} = \mathbf{a}$) results in no solutions (Figure 1(a)). The reason for this is that the partial derivatives in z-direction in $\nabla\mathbf{u}$ are zero, leading to zero determinant of both $\mathbf{V}$ and $\mathbf{W}$, and thus to the case where neither is invertible.

One way to analyze the PV problem is in terms of the cross product of the two vector fields, i.e., by analyzing where $\mathbf{v} \times \mathbf{w} = \mathbf{0}$ holds. Since the cross product is again a vector field, this requirement represents three equations, each of which defines a zero-level isosurface. Conceptually, PV solutions reside at mutual intersections of all three isosurfaces. Figure 1(a) shows these isosurfaces for our case. As can be seen, no isosurfaces are present. A more detailed inspection reveals that the first and second components of $\mathbf{u} \times \mathbf{a}$ are uniformly zero, and its third component is nonpositive. The isosurface at isolevel -2 (Figure 1(b)) indicates that this third component exhibits a ridge line, which, however, resides in general inside the cells and thus the discretized values at the cell nodes do not reach zero. Nevertheless, the field is (up to numerical error) zero along the ridge line in this configuration, and thus a PV solution. Generally, this motivates the extraction of a subset of PV solutions by means of valley lines and ridge

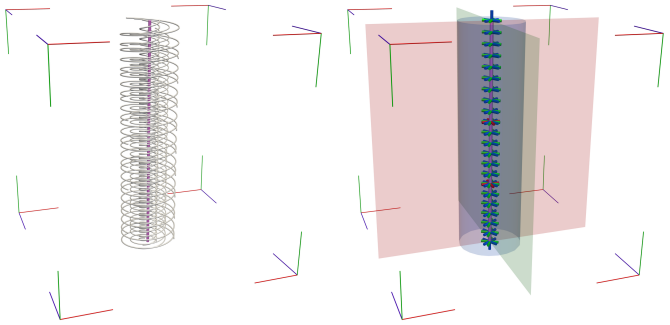

(a) (b)

Fig. 2. Straight vortex aligned with z-axis, with constant longitudinal component. (a) Streamlines (white), and ground-truth core line (purple). (b) Zero-level isosurfaces of x-component (red) and y-component (green) of $\mathbf{u} \times \mathbf{a}$. Isosurface of respective z-component at isolevel -2 (blue) indicates ridge line. Eigenvector-based approach detects only two points (red crosses). Our valley/ridge-based approach (green crosses) detects all face intersections ($\tau_\sigma = 10$), as does our subdivision-based approach (blue crosses). Please note that we depict subdivision PV solutions in blue and eigenvector-based PV solutions in red throughout this paper.

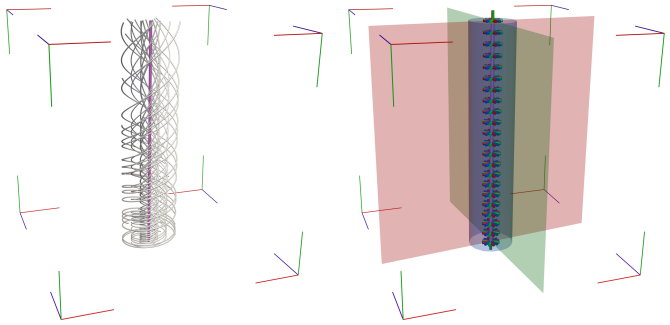

(a) (b)

Fig. 3. Same as Figure 2, but with additional linear longitudinal component. (b) All three approaches (eigenvector, ridge/valley ($\tau_\chi = 0.01$, $\tau_\sigma = 5$), and subdivision ($\tau_\chi = 0.001$, $\tau_\sigma = 10$)) find all PV face intersections for $\mathbf{u} \parallel \mathbf{a}$.

lines from the three components of $\mathbf{v} \times \mathbf{w}$. However, since only valleys and ridges where $\mathbf{v} \times \mathbf{w} = \mathbf{0}$ represent PV solutions, we need to employ filtering. We do this by rejecting those parts of these raw solution curves where $\|\mathbf{v} \times \mathbf{w}\| / \|\mathbf{v}\| / \|\mathbf{w}\|$ exceeds the user-defined threshold τ_χ. More sophisticated filtering approaches, e.g., automatic selection of τ_χ, are beyond the scope of this paper and thus subject to future work.

Please note that for extracting the valleys and ridges, we use the explicit formulation throughout this paper, i.e., instead of solving for the implicit formulation $\mathbf{g} \parallel \mathbf{H}\mathbf{g}$, we solve for $\mathbf{g} \parallel \boldsymbol{\varepsilon}$, where, for ridges, $\boldsymbol{\varepsilon}$ is the major eigenvector of $\mathbf{H}$ and the other two eigenvalues of $\mathbf{H}$ are required to be negative, and for valleys, $\boldsymbol{\varepsilon}$ is the minor eigenvector and the other two eigenvalues are required to be positive. To ensure consistency with the PV problem as defined on the quad face, we obtain $\mathbf{g}$ and $\mathbf{H}$ analytically from the bilinear interpolation function.

Notice also that, to solve for $\mathbf{v} \parallel \mathbf{w}$, we now need to solve three derived PV problems (e.g., for the first component of $\mathbf{v} \times \mathbf{w}$, we need to solve for $\mathbf{g}' \parallel \boldsymbol{\varepsilon}'$, with $\mathbf{g}' = \nabla(v_y w_z - v_z w_y)$ and $\boldsymbol{\varepsilon}'$ being the respective eigenvector of $\mathbf{H}' = \nabla \mathbf{g}'$). Unfortunately, it turns out that the eigenvector-based approach [2] also fails for this derived problem for the vortex flow under consideration. Therefore, we solve, throughout this paper, the PV problems for valleys and ridges by means of the subdivision approach presented in Section III-C. Figure 1(b) shows our respective result—in contrast to the eigenvector-based approach, we are able to obtain the complete solution.

C. PV Solution by Subdivision

Now, we add a constant longitudinal component, i.e., we use the flow from Section III-B, but set $\lambda_0 = 0.1$ (Figure 2(a)). In this configuration, the eigenvector-based approach provides only two points on the core line (red crosses in Figure 2(b)). The zero-isolevel isosurfaces of the x- and y-component of $\mathbf{v} \times \mathbf{w}$ are present, but the z-component is still nonpositive and exhibits only a ridge, which we are able to extract.

Although we are able to extract the complete solution using our ridge/valley approach, the fact that two zero-level isosurfaces intersect in this case motivates our second main contribution: obtaining PV solutions by (conceptual) intersection of zero-level isosurfaces of the components of $\mathbf{v} \times \mathbf{w}$ using subdivision. Again, to ensure consistency with the original PV problem, we formulate $\mathbf{v} \times \mathbf{w}$ by means of the analytical bilinear interpolation of $\mathbf{v}$ and $\mathbf{w}$ within the quad. If at least two of the three components of $\mathbf{v} \times \mathbf{w}$ exhibit both signs at the four corners of a (subdivided) quad, we subdivide it into four subquads and obtain the missing values of $\mathbf{v}$ and $\mathbf{w}$ by bilinear interpolation. This process is continued until less than two components exhibit both signs, or until a maximum subdivision level τ_σ is reached. Figure 2(b) shows that we obtain all PV solutions also with this approach (blue crosses).

IV. Further Evaluation

Adding to the flow from Section III-C a linear longitudinal contribution, i.e., leading to $\lambda_0 = \lambda_1 = 0.1$ (Figure 3(a)), provides sufficient variation for the eigenvector-based approach to find all solutions, as both our approaches do (Figure 3(b)).

To examine the influence of shear, we use again the flow from Section III-B, i.e., $\lambda_0 = \lambda_1 = \lambda_2 = 0$, but this time we set the shear $\sigma = 30°$ (Figure 4(a)), and $\sigma = 60°$ (Figure 4(b)). Interestingly, the eigenvector-based approach fails completely with $0°$ shear (Figure 1(b)), succeeds completely with $30°$ shear (Figure 4(a)), but then fails again almost completely with $60°$ shear (only one red cross in Figure 4(b)). In contrast, our ridge/valley-based approach succeeds in all these cases.

In the last experiment with our vortex model, we tilt the vortex from Section III-B in direction $(0, 0.47, 1)^\top$ (Figure 5). Interestingly, this causes the eigenvector-based approach to produce many solutions far away from the true solution. Since both our subdivision approach and our ridge/valley approach (which is also solved with the subdivision approach as detailed above) are based on opposite signs in only two components of $\mathbf{v} \times \mathbf{w}$ instead of all three, their solutions represent raw features that need to be filtered with τ_χ (as described above). For fair comparison, we thus filter both our PV solutions and the eigenvector-based solutions with τ_χ (although this is unusual

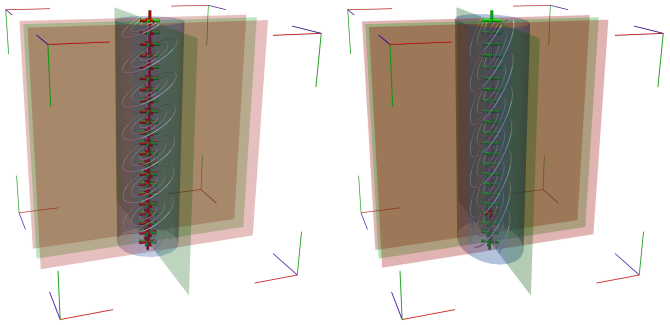

(a) (b)

Fig. 4. Same as Figure 1, but with shear of 30° (a) and 60° (b). Notice that whereas the eigenvector-based approach fails for 0° (Figure 1), it provides all PV solutions in (a) but only one solution in (b). Our valley/ridge-based approach provides all PV solutions in all these cases ($\tau_\chi = 0.001$, $\tau_\sigma = 8$).

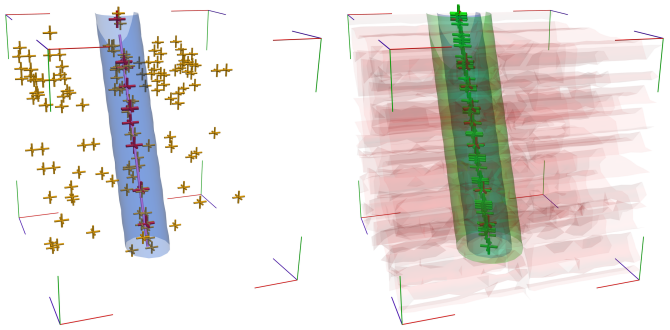

(a) (b)

Fig. 5. Same as Figure 1, but with vortex axis along $(0, 0.47, 1)^\top$. (a) Many eigenvector-based PV solutions are located away from true solution (orange). (b) Result after filtering both (a) and our ridge/valley-based raw solutions ($\tau_\sigma = 6$) with $\tau_\chi = 0.005$ shows that our approach outperforms the eigenvector-based approach. Zero-isosurface of $\mathbf{u} \times \mathbf{a}$ of x-component (red), and isosurfaces of y-component (green) and z-component (blue) at isolevel -1.

for the eigenvector-based approach), resulting in Figure 5(b). One can see that the eigenvector-based approach gives only few correct solutions in this case, too.

Last, we examine a dataset from computational geophysical fluid dynamics, representing a single time step of North Atlantic tropical storm Karl (24 Sep 2016, 00UTC). The storm was simulated using the operational forecast model (COSMO) of the German Weather Service (DWD) to study its transition into an extratropical storm, during which the storm vortex tilts and reduces its vertical extent. Figure 6(a) shows the solution of the eigenvector-based approach, which took $\mathcal{O}(10^{-1})$ s to compute. The raw (unfiltered) result of our subdivision-based approach (Figure 6(b)) took $\mathcal{O}(10)$ s with filtering and $\mathcal{O}(10^2)$ s without. The ridge/valley-based approach produced also in this case the most raw features (Figure 6(c)), which took $\mathcal{O}(10^3)$ s. We filtered both the eigenvector-based result and our raw solutions with $\tau_\chi = 2 \cdot 10^{-9}$ for comparison (Figure 6(d)), which shows that, on the one hand, only very few subdivision solutions contribute to this result, and on the other hand, some of the eigenvector-based PV solutions were of inferior quality and were therefore rejected by the filtering.

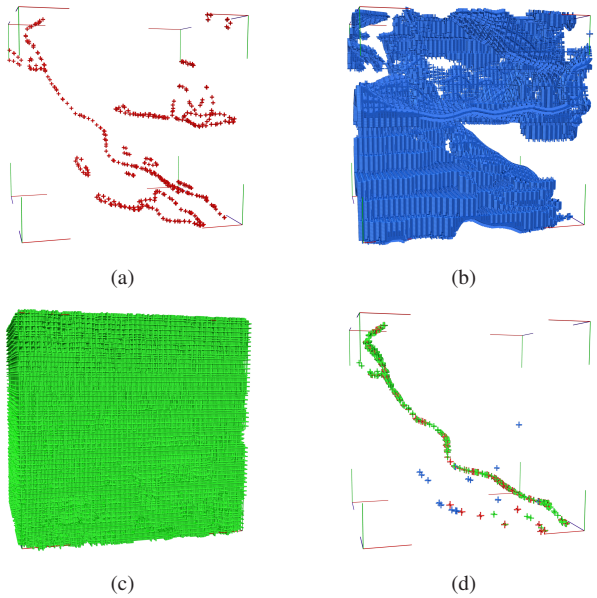

(a) (b) (c) (d)

Fig. 6. Tropical storm dataset. (a) Eigenvector-based solution. (b) Subdivision-based raw features (not filtered with τ_χ). (c) Ridge/valley-based raw features (not filtered with τ_χ). (d) Solutions from (a), (b), and (c), filtered with $\tau_\chi = 2 \cdot 10^{-9}$. Notice that some of our valley-based solutions (green) are more accurate than the eigenvector-based ones (red) and thus persist.

V. Discussion

In contrast to previous work, our approach extracts the PV solutions in all possible configurations, i.e., a) three intersecting zero-isosurfaces, b) two intersecting zero-isosurfaces (and one uniformly zero field or field exhibiting a zero-level ridge/valley), and c) at least one field exhibiting a zero-level ridge/valley (and the other(s) being uniformly zero, exhibiting a zero-level ridge/valley, or a zero-isosurface). Whereas the subdivision-based approach is typically computationally affordable, the ridge/valley-based approach tends to produce a very large number of raw features due to its "two-intersection" requirement. Although these raw features are subsequently filtered and only valid PV solutions remain, it can lead to a high computational cost. Thus, future work has to focus on reduction of raw features, possibly using early rejection tests.

VI. Conclusion

We presented a novel approach to solve the parallel vectors problem, with a focus on vortex core line extraction from vortices with vanishing longitudinal component. We identified cases where the previous approach [2] fails, and presented a solution based on subdivision with respect to the original problem and additionally its alternative formulation in terms of ridges and valleys. As future work, we would like to find an automatic approach for determining the necessary filtering threshold and better steer the subdivision [9], [10].

Acknowledgments

We thank the Transregional Collaborative Research Center SFB / TRR 165 funded by the German Science Foundation (DFG), and Lutz Hofmann for their support.

REFERENCES

[1] D. Sujudi and R. Haimes, "Identification of swirling flow in 3D vector fields," in *Proceedings of 12th AIAA Computational Fluid Dynamics Conference*, 1995, pp. 792–799.

[2] R. Peikert and M. Roth, "The parallel vectors operator: A vector field visualization primitive," in *Proceedings of IEEE Visualization*, 1999, pp. 263–270.

[3] T. Weinkauf, J. Sahner, H. Theisel, and H. C. Hege, "Cores of swirling particle motion in unsteady flows," *IEEE Transactions on Visualization and Computer Graphics*, vol. 13, no. 6, pp. 1759–1766, 2007.

[4] R. Fuchs, R. Peikert, H. Hauser, F. Sadlo, and P. Muigg, "Parallel vectors criteria for unsteady flow vortices," *IEEE Transactions on Visualization and Computer Graphics*, vol. 14, no. 3, pp. 615–626, 2008.

[5] Y. Levy, D. Degani, and A. Seginer, "Graphical visualization of vortical flows by means of helicity," *AIAA*, vol. 28, no. 8, pp. 1347–1352, 1990.

[6] J. Sahner, T. Weinkauf, and H.-C. Hege, "Galilean invariant extraction and iconic representation of vortex core lines," in *Eurographics/IEEE VGTC Symposium on Visualization*, 2005, pp. 151–160.

[7] J. Jeong and F. Hussain, "On the identification of a vortex," *Journal of Fluid Mechanics*, vol. 285, no. 69, pp. 69–94, 1995.

[8] D. Eberly, *Ridges in Image and Data Analysis*, ser. Computational Imaging and Vision. Kluwer Academic Publishers, 1996.

[9] C. Pagot, D. Osmari, F. Sadlo, D. Weiskopf, T. Ertl, and J. Comba, "Efficient parallel vectors feature extraction from higher-order data," *Computer Graphics Forum*, vol. 30, no. 3, pp. 751–760, 2011.

[10] T. Ju, M. Cheng, X. Wang, and Y. Duan, "A robust parity test for extracting parallel vectors in 3D," *IEEE Transactions on Visualization and Computer Graphics*, vol. 20, no. 12, pp. 2526–2534, 2014.